Proceedings of the Canadian Society for Mechanical Engineering International Congress 2021
CSME Congress 2021
June 27-30, 2021, Charlottetown, PE, Canada

Mixing of complex fluids: on the effects of inhomogeneity

Mohammad Reza Daneshvar Garmroodi
Dept. of Mechanical, Industrial & Aerospace Engineering
Concordia Universiy
Montreal, Quebec
mohammadreza.daneshvargarmroodi@concordia.ca

Ida Karimfazli
Dept. of Mechanical, Industrial & Aerospace Engineering
Concordia Universiy
Montreal, Quebec
ida.karimfazli@concordia.ca

***Abstract*—We investigate the time evolution of mixing in a cylindrical container that is initially stably stratified. The bottom and top halves of the container are filled with Bingham and Newtonian fluids, respectively. The mixing is promoted by a rotating disk. We consider three different disk positions and illustrate that a non-negligible steady velocity magnitude is not a sufficient condition for effective local mixing. For the model problem considered, setting the disk mixer at the middle and top of the container leads to the shortest and longest mixing times, respectively.**

***Index Terms*—Mixing, Viscoplastic fluids, Yield stress, Buoyancy.**

I. Introduction

Mixing is one of the common industrial and technological processes. Wastewater, food, and oil industries are among the examples where multiple liquids should be mixed together. In most previous studies on the mixing, working fluid is assumed to be homogeneous. In some of the homogeneous studies, mixing is evaluated using a passive concentration field. Wu [1] numerically studied the turbulent mixing of a homogeneous fluid in a container. He used a passive concentration field, and to evaluate the mixing, he defined the degree of homogeneity as follows:

$$M(x,t) = \frac{|c(x,t) - c_{avg}(t)|}{c_{avg}(t)} \times 100\% \tag{1}$$

Where $c(x,t)$ is the concentration field, and c_{avg} is the average concentration in the entire domain. He found that the mixing time is sensitive to the passive concentration field's initial position and the rheological properties of the working fluid.

It is common in studies of mixing to use the steady velocity field to identify the cavern and the dead zone. Qualitatively, the cavern is the region within the container where the fluid has a non-negligible velocity, and outside the cavern is referred to as the dead zone [2]. Mixing is considered to be negligible within the dead zone and efficient within the cavern. Pakzad et al. [3] studied both numerically and experimentally the cavern formation around a radial impeller during the mixing a Herschel-Bulkley fluid. They used velocity magnitude to define the cavern boundary. They considered 1% of the impeller tip speed for the cavern boundary's velocity, similar to what Adam [4] proposed for power-law and Newtonian fluids. In their experiments, they observed significant cavern growth during the transitional regime.

Most studies of mixing of complex fluids assume that the working fluid is homogeneous [1-6]. The variation of the fluid's properties is thus neglected in these models. In practice, mixing is often used to homogenize an otherwise inhomogeneous fluid. There are limited studies on the mixing of stratified liquids with different rheological properties. Derksen [7] numerically studied turbulent mixing of two miscible liquids with density differences in a container. He found that increasing the density difference between two liquids can impede mixing and increase the required time for complete mixing.

We consider the working fluid with a non-uniform density and rheology. The top half of the domain has a lower density and is described as a Newtonian fluid. The bottom half of the domain is filled with a viscoplastic fluid with a higher density. This initial condition can be used to model the mixing of two miscible fluids with different rheologies and densities or an inhomogeneous solution where the solute has different concentration in the top and bottom halves of the container.

We use numerical simulations to investigate the development of the flow field and the evolution of mixing when the mixer is placed at different positions. Details of the model problem and the numerical approach are discussed in section 2. In section 3 we illustrate flow features and discuss the effects of the position of the mixer. We close in section 4 by summarizing our findings.

II. Problem setup

A. Model problem

As illustrated in Fig. 1, a cylindrical tank with a rotating disk is considered as a simplified model of forced mixing in the present study. The top and bottom halves of the container are initially filled with fluid A (Newtonian fluid) and fluid B (Bingham fluid), respectively. $\widehat{r}_d, \widehat{h}_d, \widehat{R}, \widehat{h}$ and $\widehat{h}_B$ are the radius of the disk, distance of the disk from the bottom of the container, radius of the container, and height of the container and fluids interface, respectively. To reduce the computational cost, we assume that flow is axisymmetric. At top, bottom, and side walls, the no-slip boundary condition is applied.

Furthermore, the disk is assumed to rotate at a constant angular velocity ($\widehat{\Omega}$) around the z-axis.

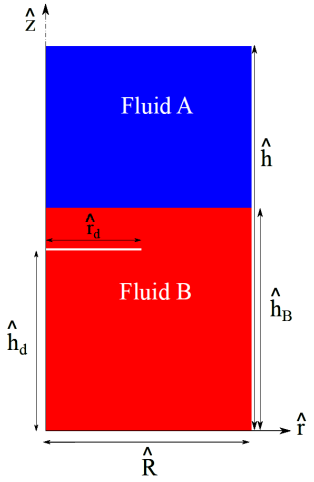

Fig. 1: Geometry in the present study

In order to model two miscible liquids, advection-diffusion equation is coupled with the Navier-Stokes equations. The non-dimensional conservation equations for momentum and concentration can be written as follows:

$$[At\alpha + 1]\left(\frac{\partial \mathbf{U}}{\partial t} + \mathbf{U}.\nabla\mathbf{U}\right) + \nabla P = \frac{1}{Re}\nabla.\boldsymbol{\tau} + Ri\,\alpha\,\mathbf{e_g} \quad (2)$$

$$\frac{\partial \alpha}{\partial t} + \nabla.(\mathbf{U}\alpha) + \frac{1}{At}\nabla.\mathbf{U} - \frac{1}{Re\,Sc}\nabla.(\nabla\alpha) = 0 \quad (3)$$

Here $\mathbf{U}, P$, and $\boldsymbol{\tau}$ represent non-dimensional velocity, pressure, and deviatoric stress tensors, respectively. α is the dimensionless concentration field such that $\alpha = 0\,(\alpha = 1)$ corresponds to pure fluid A (B), $\alpha = \dfrac{\widehat{\rho} - \widehat{\rho}_A}{\widehat{\rho}_B - \widehat{\rho}_A}$. Furthermore, $\mathbf{e_g} = (0, 0, -1)$ is the gravitational unit vector.

To obtain the non-dimensional form of the governing equations, the following dimensionless parameters are defined:

$$r = \frac{\widehat{r}}{\widehat{r}_d} \qquad z = \frac{\widehat{z}}{\widehat{r}_d} \qquad \mathbf{U} = \frac{\widehat{\mathbf{U}}}{\widehat{r}_d\,\widehat{\Omega}} \qquad t = \widehat{\Omega}\widehat{t}$$

$$P = \frac{\widehat{P}}{\widehat{\rho}_A\,\widehat{r}_d^2\,\widehat{\Omega}^2} \qquad \eta = \frac{\widehat{\eta}}{\widehat{\mu}_A} \qquad \dot{\gamma} = \frac{\widehat{\dot{\gamma}}}{\widehat{\Omega}}$$

where $\widehat{\mathbf{U}}, \widehat{P}$, $\widehat{\eta}$, and $\widehat{\dot{\gamma}}$ represent velocity, pressure, mixture viscosity, and strain rate, respectively. The dimensionless viscosity of fluid B can be written as follow:

$$\eta_B = n + \frac{Bn}{\dot{\gamma}} \quad (4)$$

where $n = \dfrac{\widehat{\mu}_B}{\widehat{\mu}_A}$ is the non-dimensional viscosity ratio. Bn is the Bingham number, which is the ratio of plastic forces to Newtonian viscous forces, and it is defined as:

$$Bn = \frac{\widehat{\tau}_y}{\widehat{\mu}_A\widehat{\Omega}} \quad (5)$$

The dimensionless mixture viscosity and shear stress are defined as follows:

$$\eta = \frac{(1-\alpha)\widehat{\mu}_A + \alpha\widehat{\eta}_B}{\widehat{\mu}_A} = (1-\alpha) + \alpha(n + \frac{Bn}{\dot{\gamma}}) \quad (6)$$

$$\tau_{ij} = \eta\,\dot{\gamma}_{ij} \quad (7)$$

At is the Atwood number, which represents the dimensionless density difference:

$$At = \frac{\widehat{\rho}_B - \widehat{\rho}_A}{\widehat{\rho}_A} \quad (8)$$

Re is the Reynolds number, which represents the ratio of inertial forces to Newtonian viscous forces,

$$Re = \frac{\widehat{\rho}_A\widehat{\Omega}\widehat{r}_d^2}{\widehat{\mu}_A} \quad (9)$$

Sc is the Shmidt number which is representative of the ratio of momentum diffusivity and mass diffusivity of the Newtonian fluid:

$$Sc = \frac{\widehat{\mu}_A}{\widehat{\rho}_A\widehat{D}_m} \quad (10)$$

and Ri represents the Richardson number which is the ratio of gravitational to inertial forces:

$$Ri = \frac{At\widehat{g}}{\widehat{r}_c\widehat{\Omega}^2} \quad (11)$$

To quantify the mixing, mixing index (MI) is defined using the standard deviation of concentration in the domain:

$$MI = 1 - \frac{\sigma}{\bar{\alpha}} \quad (12)$$

where σ is:

$$\sigma = \sqrt{\frac{1}{A}\int_A (\alpha - \bar{\alpha})^2 d_A} \quad (13)$$

Here α and $\bar{\alpha}$ are the concentration field and averaged concentration in the computational domain, respectively.

The dimensionless groups governing the model problem and the ranges considered in the current manuscript are summarized in Table. I.

TABLE I: Range of non-dimensional parameters

Non-dimensional numbers	Definition	Range
Reynolds (Re)	$\frac{\widehat{\rho}_A \widehat{\Omega} \widehat{r}_d^2}{\widehat{\mu}_A}$	10^2
Schmidt (Sc)	$\frac{\widehat{\mu}_A}{\widehat{\rho}_A \widehat{D}_m}$	10^3
Richardson (Ri)	$\frac{At\widehat{g}}{\widehat{r}_d \widehat{\Omega}^2}$	10^{-2}
Bingham (Bn)	$\frac{\widehat{\tau}_y}{\widehat{\mu}_A \widehat{\Omega}}$	10^{-1}
Atwood (At)	$\frac{\widehat{\rho}_B - \widehat{\rho}_A}{\widehat{\rho}_A}$	10^{-2}
Viscosity ratio (n)	$\frac{\widehat{\mu}_B}{\widehat{\mu}_A}$	1
Disk height (h_d)	$\frac{\widehat{h}_d}{\widehat{r}_d}$	$2-6$
Container radius (R)	$\frac{\widehat{R}}{\widehat{r}_d}$	4
Container height (h)	$\frac{\widehat{h}}{\widehat{r}_d}$	8
Fluid B height (h_B)	$\frac{\widehat{h}_B}{\widehat{r}_d}$	4

B. Numerical method

In the present study, the finite volume method has been used to discretize the governing equations. The open-source OpenFOAM toolbox has been used for the numerical solution of the equations. The numerical simulation of the problem was carried out using the "twoLiquidMixingFoam" solver. In this solver, PIMPLE or PISO-SIMPLE algorithm (Pressure-Implicit with Splitting of Operators-Semi-Implicit Method for Pressure-Linked Equations) has been used for decoupling pressure-velocity in the governing equations. In the discretization schemes, time derivatives are discretized by the first-order implicit "Euler" scheme. The divergence and gradient terms are discretized with the second-order linear "Gauss linear" scheme. Also, standard second-order central differencing "Gauss linear corrected" is used for the diffusion terms.

C. Validation

To validate our numerical solver we benchmarked our results in comparison with Huang et al. [8]. Huang et al. [8] studied laminar mixing of two miscible Newtonian liquids in a lid-driven cavity both numerically and experimentally. The schematic of their problem setup is shown in Fig. 3. The cavity is cubic with dimensions of $L \times W \times H = 5 \times 5 \times 4\,cm$, where L, H, and W are length, height, and width of the cavity, respectively. The top wall has a constant speed equal to $\widehat{U} = 0.02\frac{m}{s}$. Initially, the heights of liquid 1 and 2 are set equal to $0.75H$ and $0.25H$, respectively. The concentration colormaps of liquid 2 at different time instances are shown in Fig. 3. Comparing the present findings with Huang et al. [8] results shows a perfect agreement and our numerical solver is considered accurate.

Furthermore, four different mesh sizes are studied to verify precision. We used the finest grid (120×240) to estimate the computational error for the other grids. Table. II summarizes the results of our grid-independence studies. We have used mesh II for the rest of the simulations presented in this manuscript.

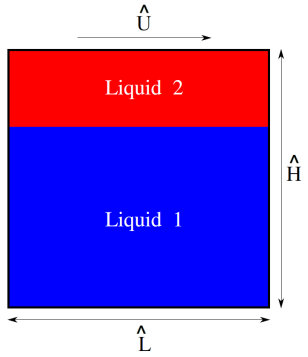

Fig. 2: Geometry in Huang et al. [8] study

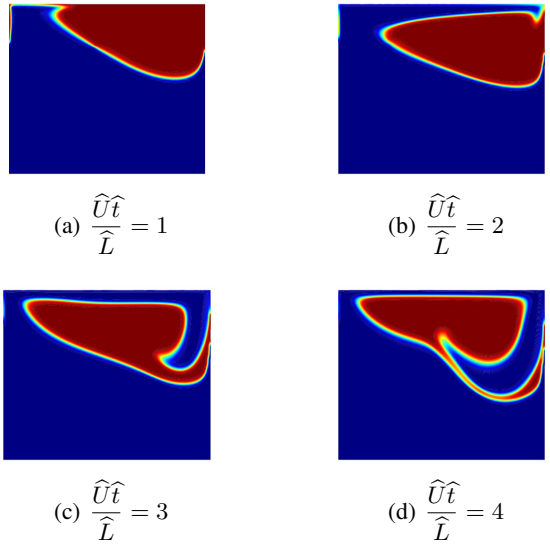

(a) $\frac{\widehat{U}\widehat{t}}{\widehat{L}} = 1$ (b) $\frac{\widehat{U}\widehat{t}}{\widehat{L}} = 2$

(c) $\frac{\widehat{U}\widehat{t}}{\widehat{L}} = 3$ (d) $\frac{\widehat{U}\widehat{t}}{\widehat{L}} = 4$

Fig. 3: Comparison of present results with [8] for $\frac{Ar}{Re} = 119, \widehat{\rho}_1 = 1307\frac{kg}{m^3}$, and $\widehat{\rho}_2 = 1297\frac{kg}{m^3}$

III. Results

An illustrative case of mixing development (at $Re = 10^2, Bn = 10^{-1}, Sc = 10^3, Ri = 10^{-2}, At = 10^{-2}, R = 4, h_d = 2, h_B = 4, h = 8, n = 1$) is shown by Fig. 4. Fig. 4a shows the initial condition where the top and bottom halves of

TABLE II: Estimated numerical error of mixing index based on different mesh sizes

($Re = 10^2, Bn = 10^{-1}, Sc = 10^3, Ri = 10^{-2}, At = 10^{-2}, R = 4, h_d = 2, h_B = 4, h = 8, n = 1, t = 12.8 \times 10^4$)

Grid	Mixing index	Error(%)
Mesh I = 60 × 120	0.6954	2.64
Mesh II = 80 × 160	0.6810	0.51
Mesh III = 100 × 200	0.6787	0.17

the container are filled with Newtonian and Bingham fluids, respectively. When the disk starts to rotate, three eddies form and mixing starts (see Fig. 4b). As time progresses, the middle eddy expands and the eddy in the top half of the container breaks down into two smaller eddies (see Fig .4c). Meanwhile, as concentration increases in the top half of the container, new unyielded regions form and grow. (Fig. 4d and 4e). Figure. 4f illustrates the evolution of mixing index. Initially, MI increases rapidly (see Fig. 4f, $t < 2\times10^4$). After the initial rapid growth, the flow reaches a quasi-steady state. The slope of MI versus time reduces and mixing is dominated by diffusion (see Fig. 4f, $t > 2 \times 10^4$).

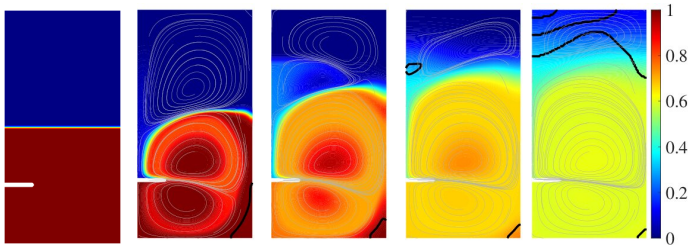

(a) $t = 0$ (b) $t = 576$ (c) $t = 6400$ (d) t=32000 (e) t=128000

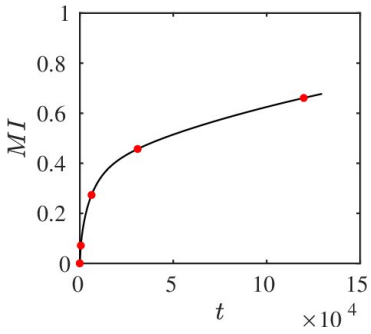

(f) Mixing index evolution

Fig. 4: Evolution of mixing at $Re = 10^2, Bn = 10^{-1}, Sc = 10^3, Ri = 10^{-2}, At = 10^{-2}, R = 4, h_d = 2, h_B = 4, h = 8, n = 1$. (a-e) Snapshots of the concentration field at different times. The gray and black lines represent the streamlines and the boundaries of the un-yielded regions, respectively. (f) Time evolution of MI.

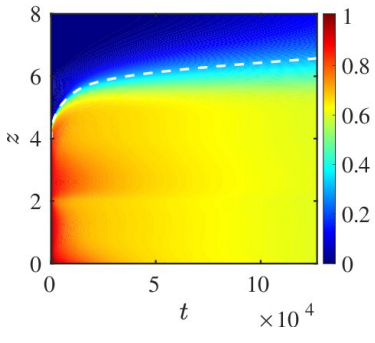

(a)

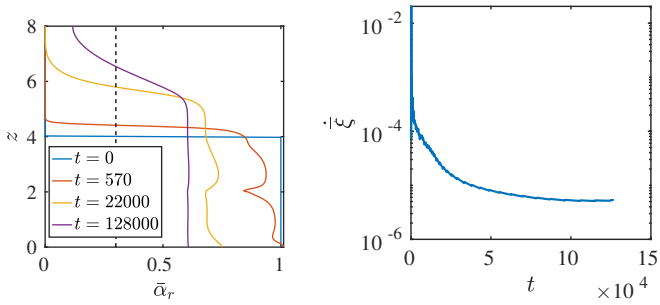

(b) (c)

Fig. 5: (a) Spatio-temporal diagram of r-averaged concentration. The dash line shows $\bar{\alpha} = 0.3$ which is used for tracking the interface of the two phases.(b) Distribution of r-averaged concentration along the z-axis in different time instances. The dash line shows $\bar{\alpha} = 0.3$. (c) The growth rate of the mixed region in the vertical direction ($Re = 10^2, Bn = 10^{-1}, Sc = 10^3, Ri = 10^{-2}, R = 4, h_d = 2, h_B = 4, h = 8, n = 1$)

Fig. 5a illustrates the spatio-temporal diagram of r-averaged concentration, $\bar{\alpha}_r(z,t)$, which is defined as follow:

$$\bar{\alpha}_r(z,t) = \frac{1}{R^2}\int_0^R 2r\alpha(r,z,t)dr \tag{14}$$

The white dash-line represents the contour $\overline{\alpha}_r = 0.3$, from hereon referred to as $\overline{\xi}$. $\overline{\xi}$ is representative of the average height of the fluids' interface above which the fluids are not mixed. It can be seen that the variation of the $\overline{\alpha}_r$ becomes slow after $t \approx 22000$. Fig. 5b shows $\overline{\alpha}_r$ distribution at different time instances. The back dash-line indicates $\overline{\alpha}_r = 0.3$. The intersection of the $\overline{\alpha}_r(t)$ and this line represent $\overline{\xi}(t)$.

Figure. 5c illustrates the time derivative of $\overline{\xi}$, i.e. $\dot{\overline{\xi}}$. $\dot{\overline{\xi}}$ illustrates the growth rate of the mixed region in the vertical direction. As can be seen, at the beginning of the mixing, the interface's speed is high. The flow then approaches a quasi-steady state, the velocity drops rapidly and stays almost constant ($t > 5 \times 10^4$).

A. *Effect of disk mixer position*

In this section, we explore the effect of the vertical position of the disk. For this purpose, three different positions have

been selected $h_d = 2, 4, 6$, from hereon referred to as the bottom, middle and top positions, respectively. Fig. 6 presents the concentration and mixing index evolution for each disk position. We consider the mixing time as time when the mixing index reaches $MI = 0.95$.

Fig. 7 illustrates the spatio-temporal diagrams of r-averaged concentration for different disk positions. Fig. 7 and Fig. 6 illustrate that when the disk is at the top and bottom positions, the fluid remains largely unmixed and the interface between high and low density regions stays almost distinct. However, when the disk is at the middle position, the interface vanishes as flow approaches the quasi-steady state. When the disk is placed in the middle of the container, fluids reach the mixed condition much faster compared to other disk positions. There is an initial rapid growth at the beginning of the mixing process for the top and bottom positions. After this initial rapid growth, the flow reaches a quasi-steady state and the diffusion mechanism dominates mixing. However, in the middle position, mixing is dominated by convection as the flow approaches a homogeneous steady-state. Mixing is thus more efficient when the disk is positioned in the middle, and has a notably shorter timescale compared to the other two cases. Furthermore, Comparing the quasi-steady states of the top, middle and bottom cases, it is evident that mixing is the least effective when the disk is at the top.

The cavern shapes in different positions are shown in Fig. 8. Fig. 8d also shows the evolution of the cavern size, V_c, for different position. Here, V_c is defined as the volume of the region where the dimensionless velocity is higher than 0.005. Also, V is the total volume of the container. The middle position has the largest cavern size compared to the bottom and top positions. A comparison of Fig8c and Fig6k reveals that the fluid is indeed not well-mixed within the cavern. This example disproves, by counterexample, that a non-negligible velocity in a part of the flow field is a sufficient condition for efficient mixing there.

IV. Conclusion

We have explored the mixing of a fluid with a non-uniform density and rheology. The top half of the domain has a lower density and is described as a Newtonian fluid. The bottom half of the domain is filled with a viscoplastic fluid with a higher density. The two fluids are considered miscible. To promote mixing, a rotating disk is placed at different vertical positions of the container.

When the disk is placed at the bottom and top positions, initially mixing progresses quickly and is dominated by advection. After this initial development, the flow reaches a quasi-steady state, and mixing is dominated by diffusion. However, for the middle position, advective mixing is more significant and the fluid reaches an approximately homogeneous quasi-steady state.

Among different positions of the disk, the middle and top positions have the shortest and longest mixing times, respectively. The interface between the high and low density regions remains relatively distinct and the fluids remain largely unmixed for the bottom and top positions compared to the middle position.

Finally, we disproved, by counterexample, that non negligible velocity indicates the areas of effective mixing. We saw that the top position had a larger cavern compared to the bottom position. However, the bottom position has a shorter mixing time compared to the top position.

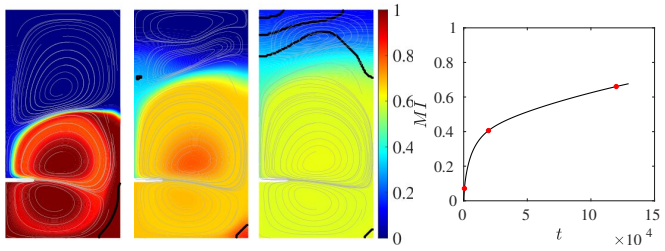

(a) $t = 576$ (b) $t = 22000$ (c) $t = 128000$ (d)

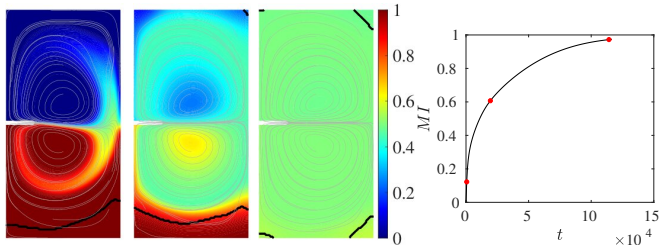

(e) $t = 576$ (f) $t = 22000$ (g) $t = 128000$ (h)

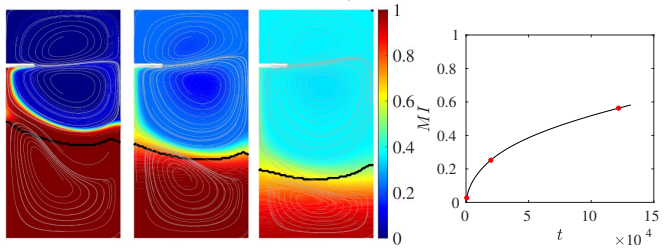

(i) $t = 576$ (j) $t = 22000$ (k) $t = 128000$ (l)

Fig. 6: Evolution of mixing at $Re = 10^2, Bn = 10^{-1}, Sc = 10^3, Ri = 10^{-2}, At = 10^{-2}, R = 4, h_B = 4, h = 8, n = 1$. (a-d), (e-h), and (i-l) are the snapshots of the concentration field at different times and mixing index evolution for bottom, middle, and top positions, respectively.

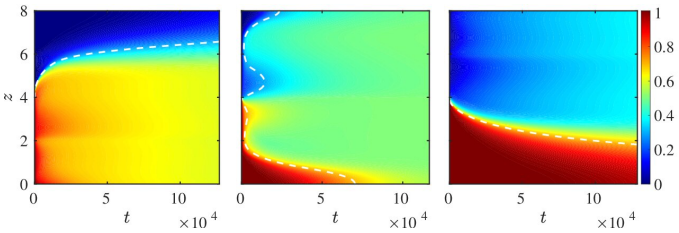

(a) Bottom (b) Middle (c) Top

Fig. 7: (a) Spatio-temporal diagram of r-averaged concentration for different disk positions.
($Re = 10^2, Bn = 10^{-1}, Sc = 10^3, Ri = 10^{-2}, R = 4, h_B = 4, h = 8, n = 1$)

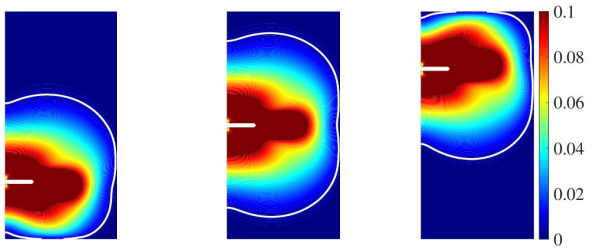

(a) bottom (b) middle (c) top

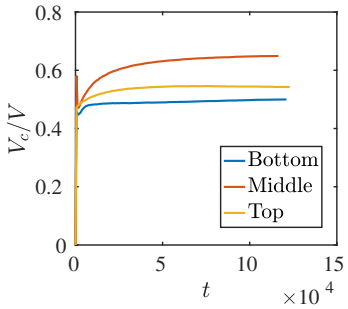

(d) Cavern evolution

Fig. 8: Evolution of cavern at $Re = 10^2, Bn = 10^{-1}, Sc = 10^3, Ri = 10^{-2}, At = 10^{-2}, R = 4, h_B = 4, h = 8, n = 1, t = 128000$. (a-c) Snapshots of the quasi-steady state velocity field at different positions. The white lines show the boundary of the cavern. (d) Time evolution of cavern in different positions.

REFERENCES

[1] Wu, B., 2010. CFD prediction of mixing time in anaerobic digesters. Transactions of the ASABE, 53(2), pp.553-563.

[2] Xiao, Q., Yang, N., Zhu, J. and Guo, L., 2014. Modeling of cavern formation in yield stress fluids in stirred tanks. AIChE Journal, 60(8), pp.3057-3070.

[3] Pakzad, L., Ein-Mozaffari, F. and Chan, P., 2008. Using electrical resistance tomography and computational fluid dynamics modeling to study the formation of cavern in the mixing of pseudoplastic fluids possessing yield stress. Chemical Engineering Science, 63(9), pp.2508-2522.

[4] Adams, L.W., 2009. Experimental and computational study of non-turbulent flow regimes and cavern formation of non-Newtonian fluids in a stirred tank (Doctoral dissertation, University of Birmingham).

[5] Boujlel, J., Pigeonneau, F., Gouillart, E. and Jop, P., 2016. Rate of chaotic mixing in localized flows. Physical Review Fluids, 1(3), p.031301.

[6] Başbuğ, S., Papadakis, G. and Vassilicos, J.C., 2018. Reduced mixing time in stirred vessels by means of irregular impellers. Physical Review Fluids, 3(8), p.084502.

[7] Derksen, J.J., 2011. Blending of miscible liquids with different densities starting from a stratified state. Computers & fluids, 50(1), pp.35-45.

[8] Huang, F., Wang, D., Li, Z., Gao, Z. and Derksen, J.J., 2019. Mixing process of two miscible fluids in a lid-driven cavity. Chemical Engineering Journal, 362, pp.229-242.